European Journal of Neuroscience, Vol. 25, pp. 2682–2696, 2007 doi:10.1111/j.1460-9568.2007.05516.x

Phasic and tonic firing properties in rat oculomotor nucleus motoneurons, studied *in vitro*

Jose Luis Nieto-Gonzalez, Livia Carrascal, Pedro Nunez-Abades and Blas Torres
Department of Physiology and Zoology, University of Seville, Avenida Reina Mercedes, 6, 41012 Spain

Keywords: firing property, membrane electrophysiology, motor system, neurophysiology in controlling eye movements, Wistar rats

Abstract

Alert-chronic studies show that ocular motoneurons (Mns) exhibit a phasic and tonic firing correlated with eye saccade-velocity and position (fixation), respectively. Differences in the phasic and tonic firing among Mns depend on synaptic inputs and/or the intrinsic membrane properties. We have used *in vitro* slice preparation to investigate the contribution of membrane properties to firing properties of Wistar rat oculomotor nucleus Mns. We recorded different discharge patterns and focused on Mns with sustained discharge (type I) because they were the most abundant, and their firing pattern resembles that reported in alert preparations. Various differences divided these Mns into types I_A and I_B; the afterhyperpolarization (AHP) phase of the spike was monophasic in I_A and biphasic in I_B; I_A Mns showed tonic or phasic-tonic firing depending on the current intensity, while I_B Mns showed phasic-tonic discharge; the phasic firing was higher in I_B than in I_A Mns; I_A Mns fired in a narrower range than did I_B Mns; and I_A Mns showed lower maximum frequency than did I_B Mns. In conclusion, I_A and I_B Mns show different phasic firing properties and dynamic range, supported by intrinsic membrane properties. We suggest that I_A and I_B Mns innervate fast-twitch muscle fibres with different contraction speeds, and could contribute to generating a fine phasic signal for a graded muscle contraction. Finally, we have demonstrated an inverse relationship between Mn thresholds and tonic firing gain, concluding that intrinsic membrane properties could not support the covariation between tonic firing gain and recruitment thresholds reported in alert studies.

Introduction

The physiological properties of Mns within the motor nuclei that generate eye movements have been characterized in both chronic and acute preparations (Grantyn & Grantyn, 1978; Delgado-Garcia *et al*., 1986; Fuchs *et al*., 1988; de la Cruz *et al*., 1989; Durand, 1989a, b; Stahl & Simpson, 1995; Sylvestre & Cullen, 1999). These Mns exhibit a tonic firing that increases with eye position (fixation) in the on-direction. The recruitment thresholds of Mns cover a wide range (e.g. in primates, from approximately 40 degrees in the off-direction to 20 degrees in the on-direction, Fuchs *et al*., 1988). The eye-position-related discharge (termed sensitivity to eye position and quantified as *K*) is distributed over a large range (e.g. in monkeys, from ~2 to ~15 spikes/s/deg) and increases with threshold (Fuchs *et al*., 1988). These Mns also exhibit a modulated spiking with slow eye movements, whose velocity sensitivity increases with threshold (Fuchs *et al*., 1988) and covaries with eye position sensitivity (Keller, 1981). The origin of eye-position-related discharges in ocular Mns remains unclear. Are the differences in *K* caused by differences in the membrane intrinsic properties (like threshold), or determined solely by differences in their afferent inputs, or a combination of the two? (Dean, 1997). In addition, ocular Mns exhibit a burst of spikes (phasic firing) correlated with saccade velocity in the on-direction, and such phasic signal is primarily provided by premotor neurons separate from those producing the tonic signal (Scudder *et al*., 2002; Sparks, 2002). Recent neuroanatomical studies suggest that two different populations of ocular Mns innervate twitch and non-twitch muscle fibres, and could drive different phasic signals (Büttner-Ennever *et al*., 2001; Eberhorn *et al*., 2006), but they have not been corroborated by physiological evidence.

Studies on Mns of the oculomotor and abducens nuclei in the brain slice preparation have shown sustained, transient, and delayed discharge patterns (Gueritaud, 1988; Tsuzuki *et al*., 1995; Russier *et al*., 2003). The firing properties have been studied in detail, using *in vitro* preparations in rodents' vestibular nucleus (reviewed in Straka *et al*., 2005), which are of particular interest here because some of these neurons are a major source of direct projections to oculomotor Mns (Carpenter, 1988). Vestibular neurons have been divided into types A and B, depending on a monophasic or biphasic afterhyperpolarization (AHP) following the action potential, and they exhibit tonic or phasic-tonic spiking (Gallagher *et al*., 1985; Serafin *et al*., 1991; Johnston *et al*., 1994; Beraneck *et al*., 2003). In view of this knowledge, we explore the following questions in the rat oculomotor nucleus Mns. First, are the different discharge patterns stated at birth and/or do they modify their frequency of appearance with age? Second, could A- or B-sustained discharge be distinguished, as in vestibular neurons? If present, could they display differences in their phasic firing properties and morphological features? Fourth, could the recordings from *in vitro* preparations help to explain whether the origin of the firing characteristics observed in alert preparation depends on intrinsic membrane properties and/or synaptic input?

Correspondence: Dr B. Torres, as above.
E-mail: btorres@us.es

J.L.N-G. and L.C. contributed equally to this work.

Received 2 January 2007, revised 23 February 2007, accepted 6 March 2007

Materials and methods

Experiments were carried out in Wistar rats (5–40 g) of both sexes, from 1 to 40 days postnatal. The experiments were performed in accord with Directive 86/609/CEE of the European Community Council, the Spanish Real Decreto 223/1988, and Seville University regulations on laboratory animal care. Rats were anaesthetized with sodium pentobarbital (50 mg/kg), and quickly decapitated. The methods to obtain the slices, recordings, and analysis are fully detailed elsewhere (Carrascal *et al*., 2006). In short, slices (300 μm) including the oculomotor nucleus were firstly incubated in a chamber containing cold sucrose-artificial cerebrospinal fluid (ACSF) for 35–45 min, and then transferred to a second chamber containing ACSF at a temperature of 21 ± 1 °C. Single slices were finally transferred to the recording chamber and superfused at 2 mL/min (Harvard, MPII) with ACSF bubbled with 95% O_2–5% CO_2 (pH 7.4; 21 ± 1 °C). The composition of ACSF was as follows (data are in mM); 126 NaCl, 2 KCl, 1.25 Na_2HPO_4, 26 $NaHCO_3$, 10 glucose, 2 $MgSO_4$, and 2 $CaCl_2$. For sucrose/ACSF solution, the 126 NaCl was substituted by 240 mM sucrose.

All recorded neurons were identified as Mns by their antidromic activation from the root of the third nerve and by the collision test (for details see Fig. 1 in Carrascal *et al*., 2006). The micropipettes used for recordings were filled with a 3 M KCl (40–70 MΩ) solution. Recordings were stored on videotape (Neuro-Corder, Neurodata Instruments, PA, USA), then played back for off-line analysis and acquired with a PCI-6070E card (National Instruments, Austin, TX, USA). All Mns included for analysis showed a stable resting membrane potential of −55 mV or more-negative, an action potential larger than 60 mV, and fired repetitively in response to supra-threshold depolarizing current steps of one second. Because this work was primarily to address characterizing the repetitive firing properties, first we identified and classified the discharge patterns in four types; sustained (or type I), transient (or type II), delayed (or type III), and discontinuously bursting (or type IV). Taking into account our previous results (Carrascal *et al*., 2005, 2006), we divided the set of recorded Mns into two main groups: neonatal (< 20-days old, $n = 97$), and adult (> 20-days old, $n = 61$). Thereafter, we focused our analysis on Mns with sustained response, as they were the most abundant. We studied these Mns in the adult period, because they exhibit mature properties that could provide functional implications in relationship with the firing rate reported in alert preparation. In addition, we investigated whether the distribution of distinct discharge patterns found in the adult was already present at birth.

We studied the characteristics of the action potential evoked by a brief current pulse (100 μs), and found two canonical action potential profiles that have been termed I_A and I_B Mns, based on their resemblance to those reported in vestibular neurons (Gallagher *et al*., 1985; Serafin *et al*., 1991; Johnston *et al*., 1994). Following the methods employed in vestibular neurons (Beraneck *et al*., 2003; Johnston *et al*., 1994), we obtained the averaged spike profile, and its first derivative and the convexity of the AHP, as quantitative methods to classify the Mns as I_A or I_B. To obtain the averaged spike profile, single action potentials evoked by depolarizing current pulses of 100 μs were averaged (eight sweeps) to measure their amplitude and duration. The amplitude was the voltage increment between the resting level and spike voltage peak. The duration of the action potential was determined as the width of the spike at its half amplitude (see also Nunez-Abades *et al*., 1993). In addition, the peak velocities of the rising and falling phases of the action potential were measured from the first derivative of the membrane potential. The averaged action potential was also used to determine the shape, amplitude, and duration of the AHP. The amplitude was the voltage increment between the resting membrane potential and the most negative value reached during the AHP. The duration was calculated as the time spent from the intersection of the repolarizing phase of the action potential with the resting membrane potential to the recovery of the resting level. According to these criteria, we divided the adult Mns with sustained firing rate into types I_A ($n = 25$) and I_B ($n = 29$).

Next, we studied the spike-frequency adaptation. The repetitive firing rate was evoked by depolarizing current steps (1 s, 0.5 Hz) with 0.05 nA increments, and shown at 0.3, 0.5, 0.7 and 0.9 nA (Table 1). We chose these currents of stimulation because at 0.3 nA all I_A and I_B Mns evoked repetitive firing throughout the current step; at 0.9 nA all I_B Mns, but only some I_A Mns (14 out of 25), were able to maintain a repetitive discharge. Further increments in current step dramatically diminished the number of firing I_A Mns. The instantaneous frequency was calculated as the reciprocal of interspike interval duration, and was plotted throughout the current step. The initial spike-frequency adaptation (Sawczuk *et al*., 1995; Rekling *et al*., 2000) was then measured. Because the instantaneous firing rate commonly showed an adaptation process that fitted a single exponential decay, we quantified the relative importance of this process by the initial adaptation index and its time course by the time constant. The initial adaptation index was equal to [1 − (frequency in the steady-steady/instantaneous frequency in the first interspike interval)]. The adaptation process calculated from this equation gave values between 0 and 1; the values 0 or 1 being pure tonic or phasic responses, respectively. The time constant of the exponential fit characterized how fast the time course of the adaptation process was. In addition, we characterized the amplitude and duration of both spike and AHP during the repetitive discharge.

We also investigated the *F/I* relationships, plotting the instantaneous frequencies of the first interspike interval or the steady-state firing frequency against the injected current. We measured the phasic and tonic components of the firing rate, defining the phasic component as

TABLE 1. Electrophysiological properties of I_A and I_B Mns of the oculomotor nucleus in response to depolarizing current steps (0.3, 0.5, 0.7 and 0.9 nA)

	I_A Mns	I_B Mns
Adaptation index		
0.3 nA	0.19 ± 0.02	0.41 ± 0.02*
0.5 nA	0.31 ± 0.03$^+$	0.52 ± 0.03*,$^+$
0.7 nA	0.46 ± 0.03$^+$	0.55 ± 0.04
0.9 nA	0.48 ± 0.04	0.57 ± 0.03
Adaptation (τ, ms)		
0.3 nA	–	62.14 ± 12.42
0.5 nA	122.98 ± 10.77$^+$	31.54 ± 5.29*,$^+$
0.7 nA	38.16 ± 3.73	32.13 ± 4.44
0.9 nA	40.89 ± 5.57	34.89 ± 4.15
Frequency/intensity (spikes/s)		
1st interspike interval		
0.3 nA	22.80 ± 1.66	33.87 ± 2.50*
0.5 nA	36.88 ± 3.71$^+$	69.35 ± 5.30*,$^+$
0.7 nA	71.65 ± 4.79$^+$	97.72 ± 3.27*,$^+$
0.9 nA	93.48 ± 7.10	123.52 ± 5.1*,$^+$
Steady-state		
0.3 nA	17.19 ± 1.03	18.87 ± 0.86
0.5 nA	23.96 ± 1.59$^+$	26.80 ± 1.51$^+$
0.7 nA	33.39 ± 2.16$^+$	40.89 ± 3.17$^+$
0.9 nA	43.54 ± 3.60$^+$	52.38 ± 3.45$^+$

Asterisks indicate significant differences ($P < 0.05$) between I_A and I_B Mns compared at equal current step (at 0.3, or 0.5, or 0.7, or 0.9 nA); crosses indicate significant differences ($P < 0.05$) between I_A or I_B Mns compared at adjacent current steps (e.g. 0.3 vs. 0.5 nA; 0.5 vs. 0.7 nA).

the instantaneous frequencies whose values were higher than those in the steady state (taken as the average value of the instantaneous frequencies during the last 500 ms of the current step). To compare the phasic or tonic components of I_A and I_B Mns, we calculated the frequency peak – obtained during the first interspike interval – and frequency in the steady state at 0.3, 0.5, 0.7, and 0.9 nA current steps. We also scored the maximum firing rate, which was defined as the highest frequency achieved by Mns before their discharge began to fail. Finally, we explored whether the slopes of the *F/I* plots in the steady state (termed 'frequency gain', Carrascal *et al*., 2006) depend on biophysical intrinsic membrane properties. With this aim, we plotted the frequency gain vs. input resistance and current threshold. We calculated the input resistance from the voltage-current plots, and we defined current threshold as the intensity of stimulating current capable of eliciting maintained repetitive firing at 15 spikes/s. This current threshold was approximately 2 × rheobase (Carrascal *et al*., 2006).

Some of the I_A and I_B Mns ($n = 11$) were intracellularly labelled. The Mns were impaled with microelectrodes filled with a solution of 2% neurobiotin (Vector Laboratories, Burlingame, CA) in 1 M KCl. Neurobiotin was iontophoretically injected by depolarizing current steps (0.5–1 nA) of 500 ms at 1 Hz for 10–60 min. After intracellular injections, the slices were transferred to a solution of 4% paraformaldehyde at 4 °C for 1–2 days, and then moved to 30% sucrose in phosphate buffer at 4 °C overnight. Thereafter, neurobiotin was revealed with the ABC kit (Vector Laboratories, Burlingame, CA, USA), following the standard methods (Nunez-Abades *et al*., 1994). Mns were reconstructed using the Neurolucida and Neuroexplorer softwares (MicrobrightField, Williston, VT, USA).

All statistical analyses were carried out on the raw data. Taking together the data of repeated measures of firing frequency and the time constant of the spike frequency adaptation on I_A or I_B Mns, first we determined if there were significant differences at several different current intensities, using a one-way ANOVA test. If there were significant differences, we used the Bonferroni test to perform pairwise comparisons between groups, and the significance level was $P < 0.05$. Two sets of comparisons were carried out; first, between data of I_A and I_B Mns at equal current intensity (at 0.3, or 0.5, or 0.7, or 0.9 nA); second, between data belonging to I_A or I_B Mns taken at adjacent steps of current intensity (e.g. 0.3 vs. 0.5 nA; 0.5 vs. 0.7 nA…). Finally, mean ± standard error was calculated for each parameter.

Results

All recorded Mns of the oculomotor nucleus were silent at their resting membrane potential, and required supra-threshold depolarizing current steps to evoke a repetitive firing. We classified the Mns into four types, depending on their percentage of appearance and discharge pattern, type I (or sustained); type II (or transient); type III (or delayed); and type IV (or discontinuously bursting; Fig. 1). Type I Mns were the most abundant in both the neonatal ($n = 90/97$, 92.8%) and adult ($n = 54/61$, 88.5%) periods. They showed a sustained discharge throughout the current step (Fig. 1A), and their firing rate shifted with the current intensity (Fig. 1B). Type II Mns ($n = 6$, four being in the adult period) generated up to six spikes as long as 300 ms after the stimulus onset, and then failed to discharge (Fig. 1C); the number of spikes varied with the current step (Fig. 1D); the successive spikes decreased in amplitude and increased in duration. Type III Mns ($n = 3$) were confined to the neonatal period, and discharged with a considerably delayed first spike after weak current steps (Fig. 1E); the latency of the first spike decreased with the increase in the current intensity (Fig. 1F), and after the first spike, the discharge was sustained, ending with stimulation. Commonly, the firing rate increased for first, second, and third interspike intervals, then reached a constant frequency. Type IV Mns ($n = 2$ and three for neonatal and adult periods, respectively) discharged bursts of spikes distributed discontinuously throughout the step (Fig. 1G); the number of bursts and the time between them depended on the current intensity (Fig. 1H); current steps higher than 0.5 nA yielded a sustained spiking (not illustrated). Because most of the Mns showed a sustained response, and this firing pattern resembles that reported in the alert preparation of adult subjects (see Introduction), we focused our analysis in this study on the repetitive firing properties of type I adult Mns.

Action-potential shape

The Mns with sustained discharge were, in turn, divided into I_A and I_B, depending on the features of the action-potential shape evoked by a brief depolarizing current pulse (see question 2 in the Introduction section). The I_A Mns showed a single deep AHP (Fig. 2A), while I_B Mns showed an early fast AHP and a delayed slow AHP (Fig. 2B). In addition, an afterdepolarization phase was observable in I_B Mns (Fig. 2B). In the adult period, I_A (25/54) and I_B (29/54) Mns were similarly distributed; while in the neonatal epoch, I_A Mns were more frequent (85/90). The amplitude of the action potential was similar for I_A (62.5 ± 1.8 mV) and I_B (63.5 ± 1.6 mV) adult Mns, while its duration was significantly longer for the former ($I_A = 1.28 \pm 0.05$ ms; $I_B = 1.16 \pm 0.05$ ms; Fig. 2C and D). In addition, the rising phases showed similar instantaneous peak velocities for I_A (115.8 ± 8.8 V/s) and I_B (120.8 ± 8.1 V/s) Mns; however, the falling phases were faster for I_B Mns (in the case illustrated in Fig. 2E, 11 V/s) than for I_A Mns. This difference was significant ($I_A = 58.7 \pm 4.1$ V/s and $I_B = 72.2 \pm 5.5$ V/s).

As indicated, I_A and I_B Mns showed monophasic and biphasic AHP, respectively (Fig. 2A and B), which had similar amplitude ($I_A = 6.71 \pm 0.65$ mV and $I_B = 5.74 \pm 0.35$ mV) and duration ($I_A = 101.1 \pm 8.2$ ms and $I_B = 96.5 \pm 4.2$ ms). In addition, the AHP had concave and convex voltage traces in I_A and I_B Mns, respectively (Fig. 2F and H). The first-derivative function of the AHP in I_A Mns showed a single transient positive component (Fig. 2G). The double component of the AHP in I_B Mns was observed in its first-derivative function as a pronounced positive voltage trace followed by another, transient negative decrease in the rate of depolarization (Fig. 2I). Finally, we found differences in the repetitive firing properties between I_A and I_B Mns of the rat oculomotor nucleus. These differences were studied in terms of spike-frequency adaptation and action-potential features during the repetitive discharge. In addition, we studied the phasic response of I_A and I_B Mns determined by equal amplitude current steps, and the tonic response from *F/I* plots to investigate whether their slopes (firing rate gain) depend on input resistance and current threshold.

Spike-frequency adaptation

Figure 3A and B illustrates two representative examples of the repetitive firing for I_A and I_B Mns evoked by current steps of 0.3 and 0.9 nA. The I_A Mn exhibited an essentially tonic discharge (without adaptation) at 0.3 nA. Thus, the duration of the first interspike interval (left in Fig. 3A, *) was similar to those in the steady state. With 0.9 nA, the response shifted to phasic-tonic, as the first interspike interval (right in Fig. 3A, *) was shorter than those in the steady state.

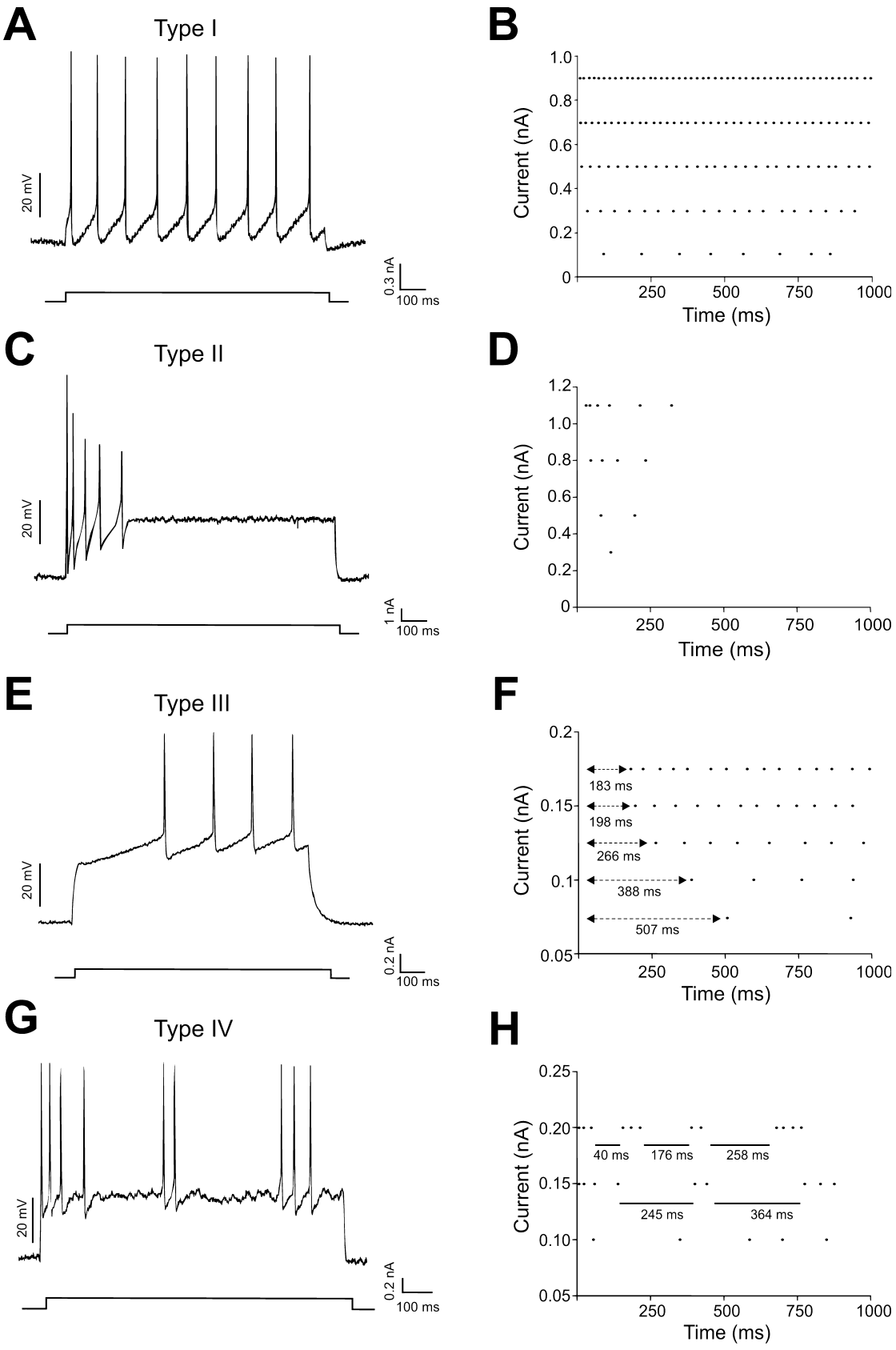

FIG. 1. Discharge patterns in motoneurons (Mns) of the rat oculomotor nucleus. (A, C, E and G) Time course of the spikes evoked by supra-threshold depolarizing current steps in Mns with sustained (type I), transient (type II), delayed (type III), and discontinuously bursting (type IV) firing. (B, D, F and H) Dot-raster, showing responses of each Mn type to different current intensity. Each dot represents a single action potential. In F, durations indicate the gap between stimulus onset and the first spike, and in H, the gap between bursts of spikes.

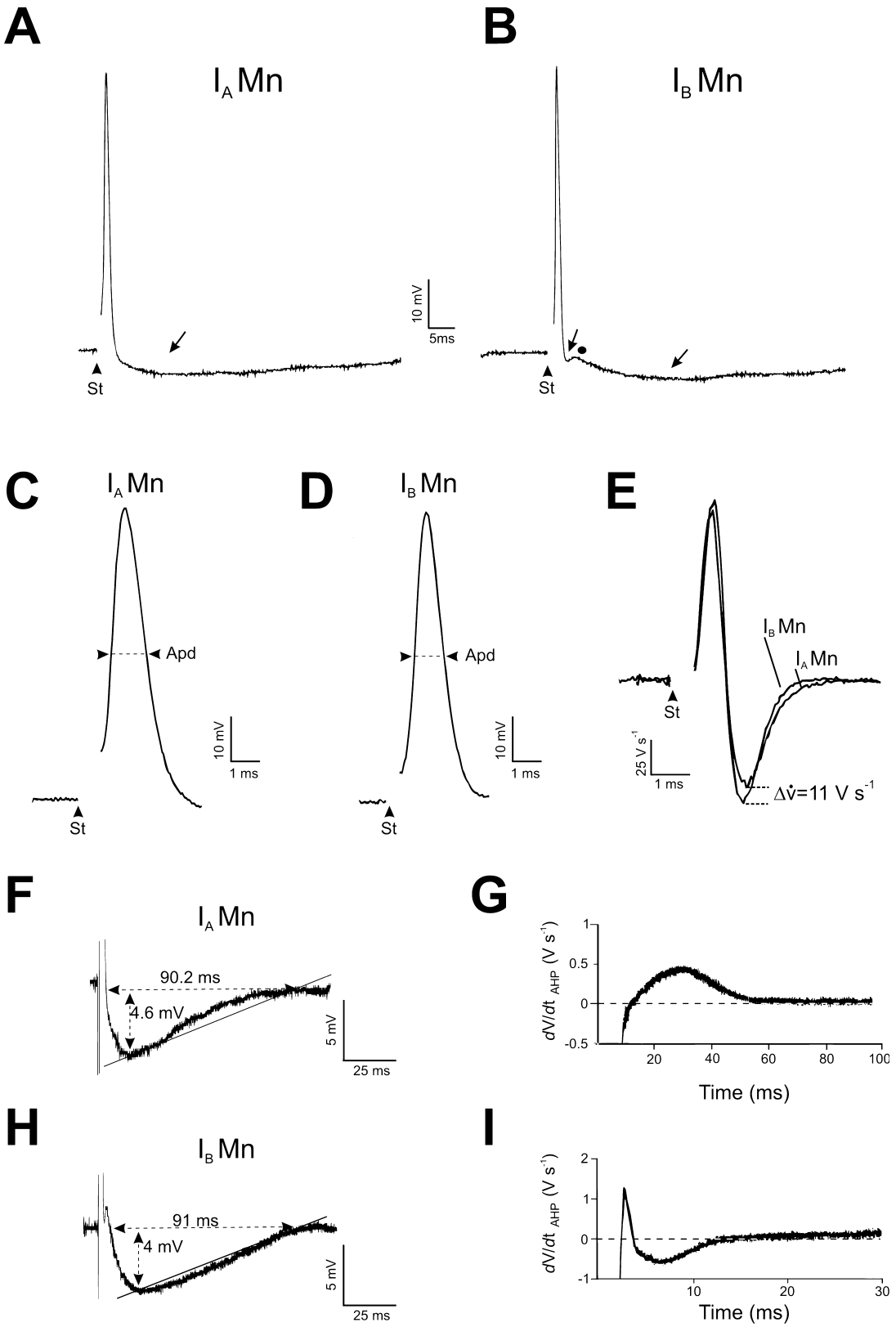

FIG. 2. Characteristics of the action-potential shape in I_A and I_B motoneurons (Mns) of the rat oculomotor nucleus. (A and B) Two representative action potentials of I_A and I_B Mns evoked by brief depolarizing current pulses (100 μs). Arrowheads indicate the onset of stimulus. I_A Mns showed a single deep afterhyperpolarization phase (AHP, ↓). I_B Mns showed an early fast AHP (↓), a delayed slow AHP (↓), and afterdepolarization phase (●). (C and D). Action-potential duration (Apd) and amplitude in I_A and I_B Mns. (E) First-derivative function of the action potentials represented in A and B, emphasizing the difference in the instantaneous velocity of the falling phase. (F and H) Afterhyperpolarization phases of the Mns illustrated in A and B. Dashed lines indicate duration and amplitude of the AHP, while solid lines join the AHP voltage peak with the return to baseline. (G and I) First-derivative function of the AHP phases represented in F and H.

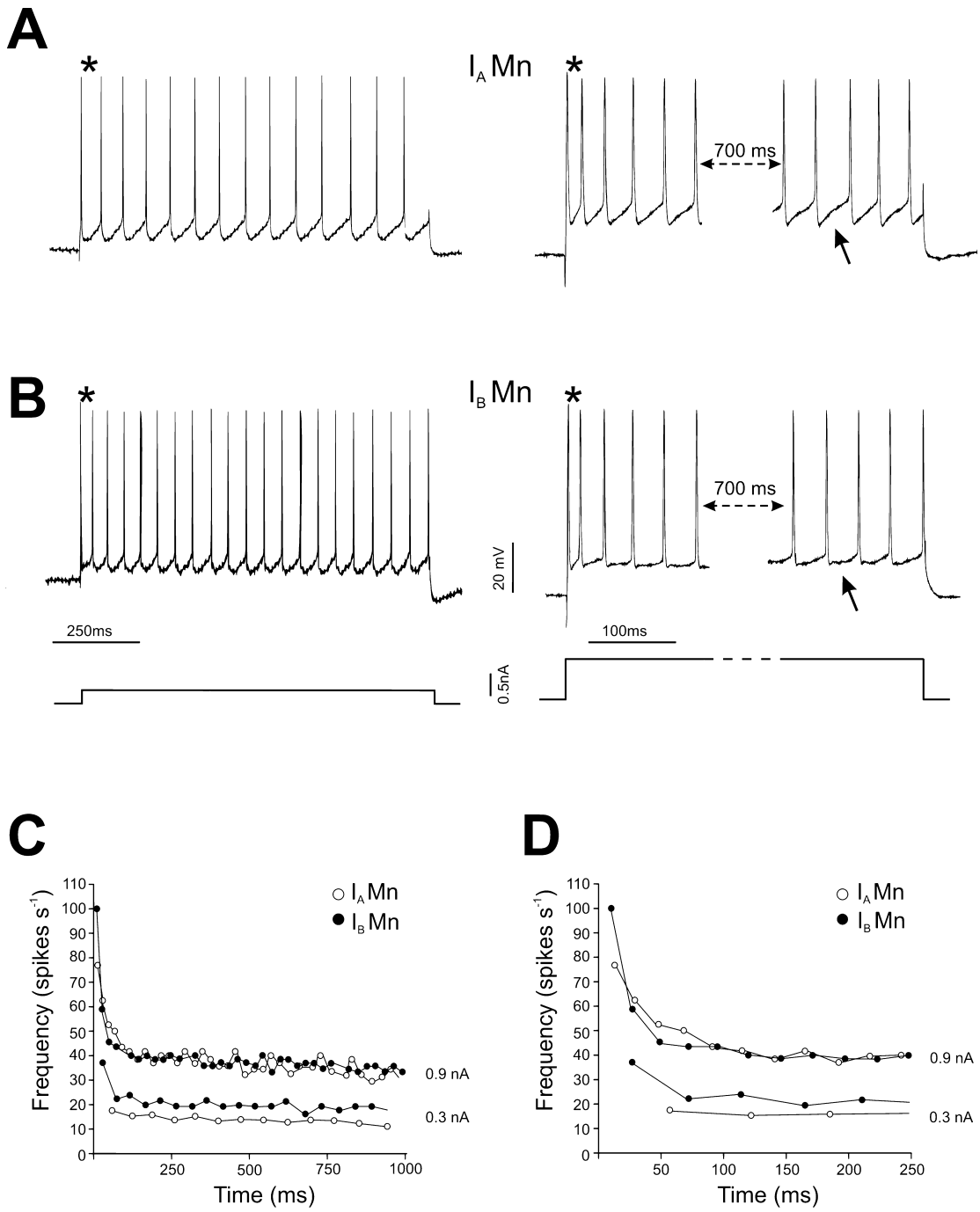

FIG. 3. Repetitive discharge in I_A and I_B motoneurons (Mns) of the rat oculomotor nucleus. (A and B) Repetitive discharge evoked by depolarizing current steps (1 s) at 0.3 and 0.9 nA in I_A and I_B Mns. Asterisks indicate the first interspike interval, and arrows show the time course of the afterhyperpolarization phase. (C and D) Plots representing the instantaneous frequency of the Mns illustrated in A and B in response to different intensities of stimulation (0.3 and 0.9 nA) for 1 s (C) and the first 250 ms (D) after stimulus onset.

A phasic-tonic firing was observed for all I_B Mns through the whole range of stimulation (Fig. 3B). These observations were consistent with those obtained from the plots of the instantaneous frequencies against the time in which the stimulus was on (Fig. 3C and D). As shown, the current step of 0.3 nA evoked a constant frequency in the I_A Mn, but not in the I_B – for which the highest frequency was in the first interspike interval and then decayed until reaching a steady state. In contrast, 0.9 nA evoked a phasic-tonic response in both I_A and I_B Mns. The time course of the phasic-tonic responses were fit with a single exponential ($r > 0.7$).

The initial adaptation index quantified the relative importance of the spike-frequency adaptation process (Table 1). The adaptation index scored at 0.3 nA current steps comprised a continuum from 0.03 to 0.68, but its distribution range was shifted between I_A and I_B Mns (Fig. 4A). As shown in Fig. 4B, adaptation indexes between 0.03 and 0.2 included only I_A Mns (12/25). Adaptation indexes between 0.2 and 0.4 included both I_A (13/25) and I_B (14/29), and between 0.4 and 0.7 only I_B Mns (15/29) (Fig. 4A and B). The adaptation indexes were significantly different between I_A and I_B Mns at 0.3 and 0.5 nA (Table 1). These data demonstrated that (at

currents up to 0.5 nA) I_A Mns exhibited an almost pure tonic firing, in particular for those Mns with an adaptation index below 0.2, while I_B Mns discharged with phasic-tonic spiking. In contrast, the adaptation index scored at 0.7 and 0.9 nA was not significantly different for I_A and I_B Mns (Table 1), indicating that both populations of Mns exhibited a phasic-tonic firing. In fact, the adaptation index increased significantly with current intensity until reaching plateau values of approximately 0.5–0.6 in both I_A and I_B Mns (Fig. 4A and C; Table 1). At 0.9 nA current steps, most of the Mns showed an adaptation index overlapping in the same range, between 0.3 and 0.7 ($I_A = 13/14$; $I_B = 23/29$), the remainder being shifted towards lower or higher values for I_A and I_B Mns, respectively (Fig. 4A and C). In summary, these data showed an essentially tonic or phasic-tonic discharge rate in I_A Mns as a function of the current intensity, while it was always phasic-tonic in I_B Mns through the whole range of stimulation. We also measured the time course of the initial spike-frequency adaptation by the time constant of the exponential fit. There were two main results; first, the time constant diminished with increases in the current intensity, reaching plateau values of approximately 30–40 ms for both I_A and I_B Mns; and second, the time constant was significantly lower in I_B (i.e. adapted faster) than in I_A Mns at currents equal to 0.5 nA, but no difference was scored at higher currents (Table 1).

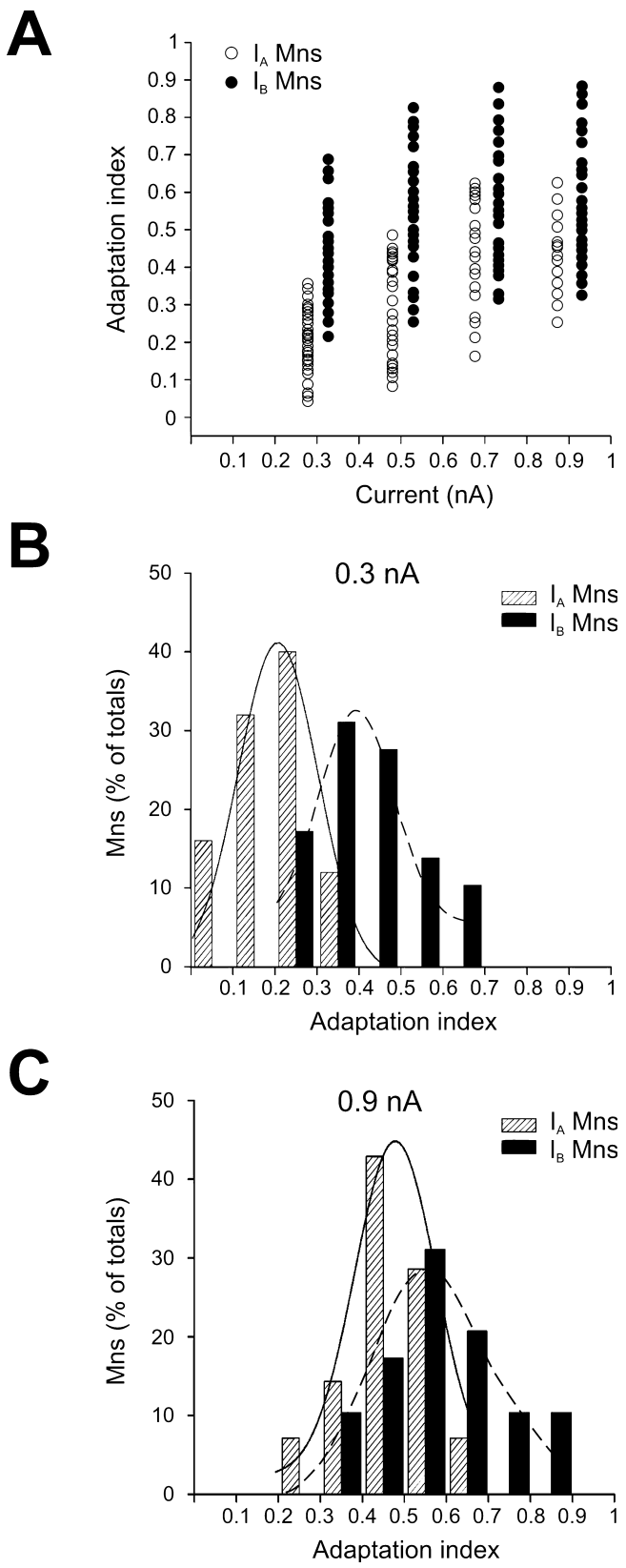

Action-potential shape during the repetitive discharge

Figure 5 compares the action-potential shape for the first spike and those in the steady state during the repetitive discharge. As shown, I_A and I_B Mns showed spike amplitude and duration similar across the repetitive firing (Fig. 5A and B). However, there were significant differences between I_A and I_B Mns in spike duration ($I_A = 1.02 \pm 0.006$ ms and $I_B = 0.97 \pm 0.008$ ms), but not in spike amplitude (approximately 63 mV). The AHP shape of I_A and I_B Mns was different not only when evoked with a brief depolarization pulse (see Fig. 2F and H), but also during the repetitive discharge (Fig. 3A and B). Figure 5C–F compares the AHP features in I_A and I_B Mns at two different current intensities. For I_A Mns, at 0.3 nA (Fig. 5C), AHP amplitude (8.6 ± 0.6 mV) and duration (49.2 ± 5.6 ms) following the first spike were similar to those in the steady state (amplitude $= 9.1 \pm 0.7$ mV; duration $= 61.8 \pm 4.3$ ms), but at 0.9 nA (Fig. 5E) they were significantly different (5.1 ± 0.2 mV vs. 8.2 ± 0.9 mV; and 11.0 ± 2.2 ms vs. 21.6 ± 3.1 ms). In contrast, and irrespective of the current intensity, in I_B Mns (Fig. 5D and F), AHP amplitude (5.4 ± 0.6 mV and 5.1 ± 0.6 mV at 0.3 and 0.9 nA, respectively) and duration (34.4 ± 5.2 ms and 9.3 ± 0.8 ms at 0.3 and 0.9 nA, respectively) following the first spike were different from those in the steady state (6.8 ± 0.5 mV and 6.4 ± 0.6 mV at 0.3 nA and 0.9 nA, respectively; 57.18 ± 5.10 ms and 20.19 ± 2.15 ms at 0.3 and 0.9 nA, respectively). All of these differences were significant. In the steady state, AHP amplitude was significantly higher (see data above) in I_A than in I_B Mns, whereas the duration was similar.

FIG. 4. Spike-frequency adaptation in I_A and I_B motoneurons (Mns) of the rat oculomotor nucleus. (A) Plot representing the raw data of adaptation index vs. current intensity. Data are illustrated at 0.3, 0.5, 0.7, and 0.9 nA; those from I_A Mns (open circles) and I_B Mns (filled circles) are shown separately to avoid overlapping. (B and C) Histograms showing the distribution of the adaptation index calculated at 0.3 and 0.9 nA for I_A (dashed bars) and I_B (solid bars) Mns. The percentage of Mns corresponding to the ordinate axis was equal to [(number of Mns with an adaptation index in a range/total number of I_A or I_B Mns) × 100]. The solid and dashed lines depicted in B and C corresponding to Gaussian fit for the distributions of I_A and I_B Mns, respectively.

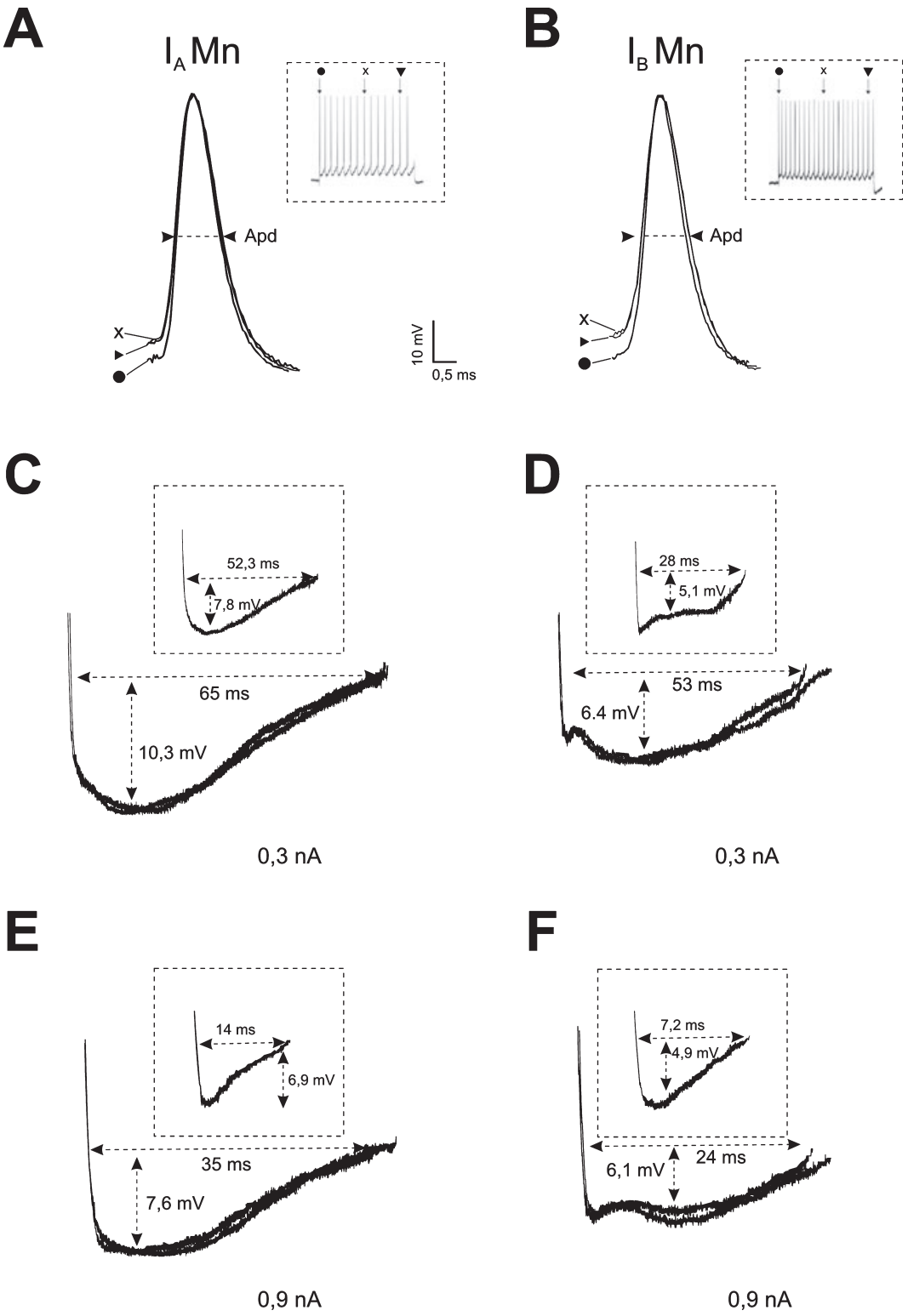

FIG. 5. Action-potential features during repetitive discharge in I_A and I_B motoneurons (Mns) of the rat oculomotor nucleus. (A and B) Three action potentials aligned on peak voltage taken from beginning (●), middle (▶), and end (x) of the repetitive discharge (see, in the insets, their correspondence in the train of spikes). (C, D, E and F) Afterhyperpolarization phases (AHP) following the action potentials of the I_A (C and E) and I_B (D and F) Mns taken at 0.3 and 0.9 nA. The insets depict the AHP that followed the first spike.

F/I plots

Frequency of the first interspike interval and steady state are dependent upon current intensity in both I_A and I_B Mns (Fig. 6A and B; Table 1). As shown in Fig. 6C and D, the frequency of the first interspike interval was distributed in a continuum, ranging between 10 and 50 spikes/s with stimulation of 0.3 nA, and from 40 to 220 spikes/s at 0.9 nA. However, the distributions of the instantaneous

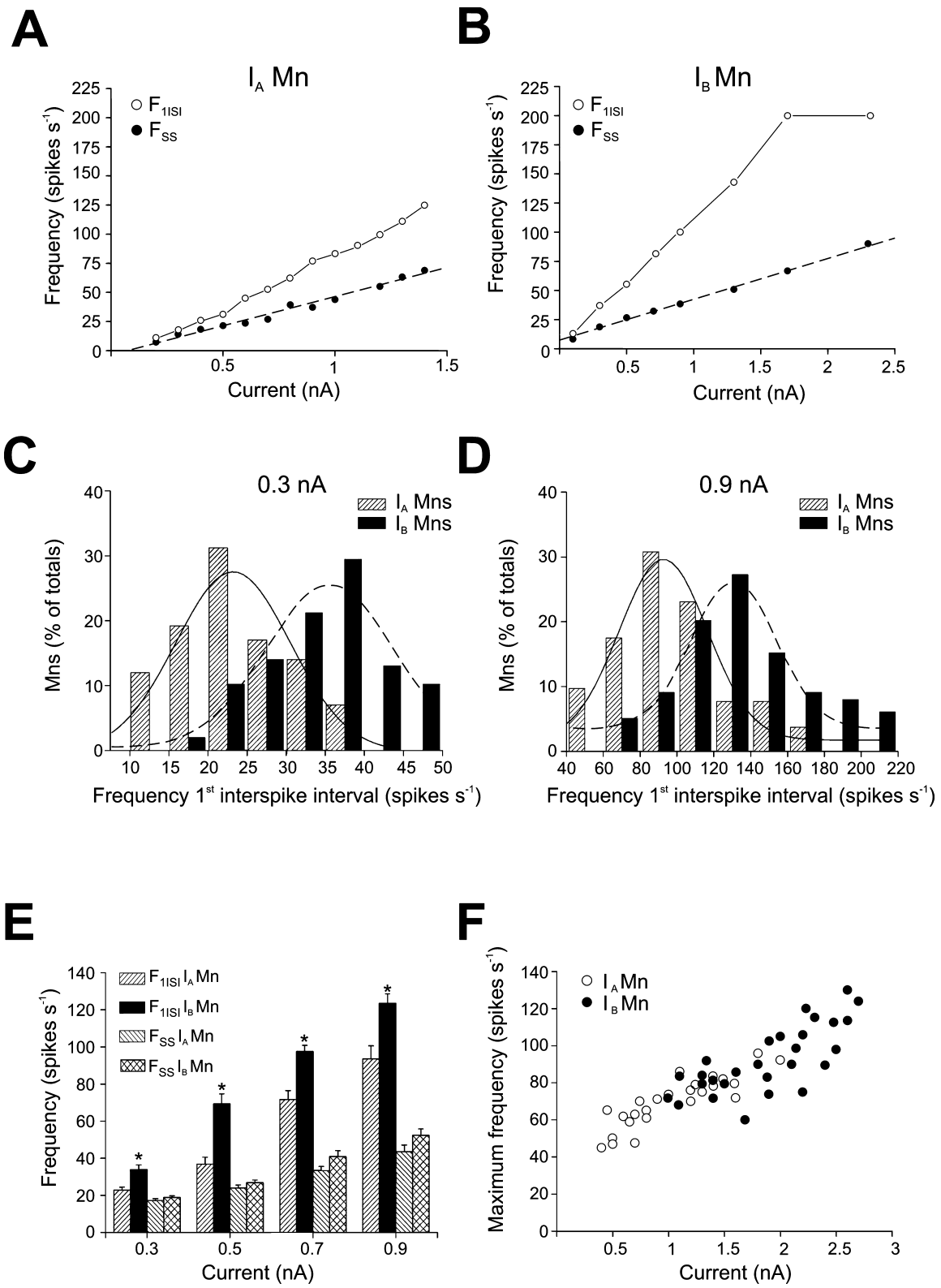

FIG. 6. Frequency of discharge as function of the current intensity of stimulation in I_A and I_B motoneurons (Mns) of the rat oculomotor nucleus. (A and B) Plot of the instantaneous frequency for the first interspike interval (F_{1ISI}) and the steady state (F_{SS}) in two representative I_A and I_B Mns. The instantaneous frequency for the first interspike interval is connected by lines. The dashed lines illustrate the best fit to the raw data for the frequency in the steady state (the slope indicates the frequency gain). (C and D) Histograms showing the distribution of F_{1ISI} scored at 0.3 and 0.9 nA in I_A (dashed bar) and I_B (solid bar) Mns. The percentages of Mns on the ordinate axis were equal to [(number of Mns whose F_{1ISI} was included in each interval of the abscissa axis/total number of I_A or I_B Mns) × 100]. The solid and dashed lines correspond to Gaussian fit for the distributions in I_A and I_B Mns. (E) Histogram illustrating the mean and standard errors of F_{1ISI} and F_{SS} at four different currents of stimulation in I_A and I_B Mns. Asterisks indicate significant differences between F_{1ISI} in I_A and I_B Mns (for further statistical comparison, see Table 1). (F) Relationship between the maximum frequency and the current at which it was reached for I_A and I_B Mns.

frequency for the first interspike interval were shifted between I_A and I_B Mns, always being significantly higher in I_B than in I_A Mns (Table 1). No significant differences were found between the instantaneous frequency of the first interspike interval and that in the steady state in I_A Mns stimulated at currents up to 0.5 nA. However, with larger current steps, these frequencies were significantly different (Fig. 6A and E; Table 1). In contrast, I_B Mns showed significant differences in the instantaneous frequencies of the first interspike interval and those in the steady state across the whole range of current steps (Fig. 6B and E; Table 1). Furthermore, irrespective of the current intensity, no significant differences were found for the frequencies of the steady state between I_A and I_B Mns (Fig. 6E; Table 1). In summary, we demonstrated the phasic component to be systematically higher in I_B than in I_A Mns. Finally, the dynamic range of supra-threshold depolarizing current steps in which the Mns could modulate the firing rate was narrower for I_A (0.1–2 nA) than for I_B Mns (0.05–3 nA).

Figure 6F illustrates the maximum of the repetitive discharge against the current required to reach such a firing rate for I_A and I_B Mns. The Mns reached their maximum firing rate across a continuous range of current between 0.5 and 3 nA; these stimulations led to maximum frequencies that were also distributed in a continuum between 50 and 130 spikes/s. However, the functional ranges for I_A and I_B Mns were shifted. Thus, I_A Mns reached the maximum discharge in response to current steps that ranged between 0.5 and 2 nA, while for I_B Mns, the range was between 1 and 3 nA. In fact, we never recorded I_A Mns that increased their discharge in response to stimulations higher than 2 nA, nor did we find I_B Mns that failed to maintain their repetitive discharge with current steps lower than 1 nA. Consequently, the maximum firing rate for I_A Mns ranged between 50 and 90 spikes/s, while that for I_B Mns ranged between 75 and 130 spikes/s; we never found I_A Mns whose maximum frequency was higher than 90 spikes/s, and type I_B Mns were always above 75 spikes/s.

Morphometrical analysis

This section of the study investigates whether I_A and I_B Mns can be distinguished in anatomical terms. Figure 7A–D illustrates two electrophysiologically representative I_A and I_B Mns (see insets in Fig. 7A and C) lying within the oculomotor nucleus. These Mns showed similar somata shape (Fig. 7A and C) and dendritic tree (Fig. 7B and D). In fact, the morphometrical data of I_A ($n = 6$) and I_B ($n = 5$) Mns recovered after intracellular injections of neurobiotin did not reveal clear-cut differences between them. Thus, all I_A and I_B Mns had polygonal or spherical cell bodies with similar size [(maximum + minimum cell diameters)/2] for I_A Mns (22.5 ± 1.9 μm) and I_B Mns (20.7 ± 2.1 μm) and a number of main dendrites ranging between 4 and 7. Attending to the location, I_A and I_B Mns were intermingled within the boundaries of the oculomotor nucleus (Fig. 7E). Finally, to check whether the passive membrane properties covary with the size of the Mns, we plotted input resistance vs. the somato-dendritic surface and found a significant linear regression between them ($P < 0.05$; $r = -0.5$; Fig. 7F).

F/I plots vs. intrinsic membrane properties

We checked if the intrinsic membrane properties could determine the slope of the *F/I* plots. With this aim, we first determine whether I_A and I_B Mns were distinct in some of their intrinsic membrane properties. There was no significant difference in resting membrane potential ($I_A = -61.4 \pm 2.9$ mV and $I_B = -62.6 \pm 2.8$ mV) or input resistance ($I_A = 56.1 \pm 2.4$ MΩ and $I_B = 52.8 \pm 2.7$ MΩ). Furthermore, I_A and I_B Mns had similar frequencies in the steady state (Fig. 6E and Table 1). Consequently, the slopes of the *F/I* linear regression appeared intermingled (Fig. 8A, solid and dashed lines correspond to I_A and I_B Mns, respectively), and no significant differences in frequency gain (slopes of these *F/I* linear regressions) could be established between I_A (52.1 ± 4.6 spikes/s/nA) and I_B (53.8 ± 3.2 spikes/s/nA) Mns. No difference was found in the current threshold, being 0.25 ± 0.02 nA in I_A Mns and 0.24 ± 0.01 nA in I_B Mns. In addition, neither input resistance nor current threshold significantly depended on resting membrane potential. All these data together allowed us to collapse the raw data of I_A and I_B Mns to test whether the frequency gain of the repetitive discharge in the steady state depended on intrinsic membrane properties (Fig. 8C and D). Even though the raw data were taken as a single pool, we represented them differently for I_A and I_B Mns, to provide evidence that no separation was observable when we plotted the frequency gain vs. input resistance or current threshold. Figure 8B illustrates Mns with similar resting membrane potentials whose *F/I* slopes were the lowest and highest found. As can be observed, the Mn with the higher *F/I* slope (termed frequency gain elsewhere, Carrascal *et al*., 2006) also had a higher input resistance and lower current threshold. We studied whether these qualitative observations could be extended to the whole motoneuronal pool. The values of frequency gain covaried positively with input resistance (Fig. 8C). This linear regression was significant but poorly fitting ($P < 0.05$; $r = 0.35$). In addition, we found a significant and more robust negative correlation between frequency gain and current threshold ($P < 0.001$; $r = -0.6$; Fig. 8D).

Discussion

This work has demonstrated the presence of four different patterns of repetitive discharge in the Mns of the oculomotor nucleus; sustained (type I), transient (type II), delayed (type III), and discontinuously bursting (type IV). We will discuss in detail type I Mns because they had phasic and tonic firing, were the most abundant, and their repetitive discharge was similar to that reported in alert preparations. Before that, we will discuss some technical considerations of the method.

Technical considerations of the method

Lower temperature than physiological is routinely used for experimentation *in vitro* (Nunez-Abades *et al*., 1993; Sawczuk *et al*., 1995; Magarinos-Ascone *et al*., 1999; Carrascal *et al*., 2006; present data). Reduced temperature may enhance slice viability and increase the dissolved oxygen content of the bathing medium (Thompson *et al*., 1985). Cooling slows ionic conductance kinetics and diminishes linearly firing rate; rewarming the cell reverses these effects (Thompson *et al*., 1985; Burgoon & Boulant, 2001; Zhao & Boulant, 2005). In monkeys, ocular Mns can fire up to 400 Hz (Fuchs & Luschei, 1971), while the maximum frequency reported here reached ∼130 spikes/s. These differences could be a consequence of temperature, experimental conditions, and/or species-specific features. However, we can safely rule out the former two because the range of firing rate reported here is similar to that recorded from acute preparation in rat oculomotor Mns (Durand, 1989b). Furthermore, the time constants of the spike frequency adaptation plots were similar to those reported from acute preparation of cat ocular Mns injected with current steps (Remmel & Marrocco, 1975).

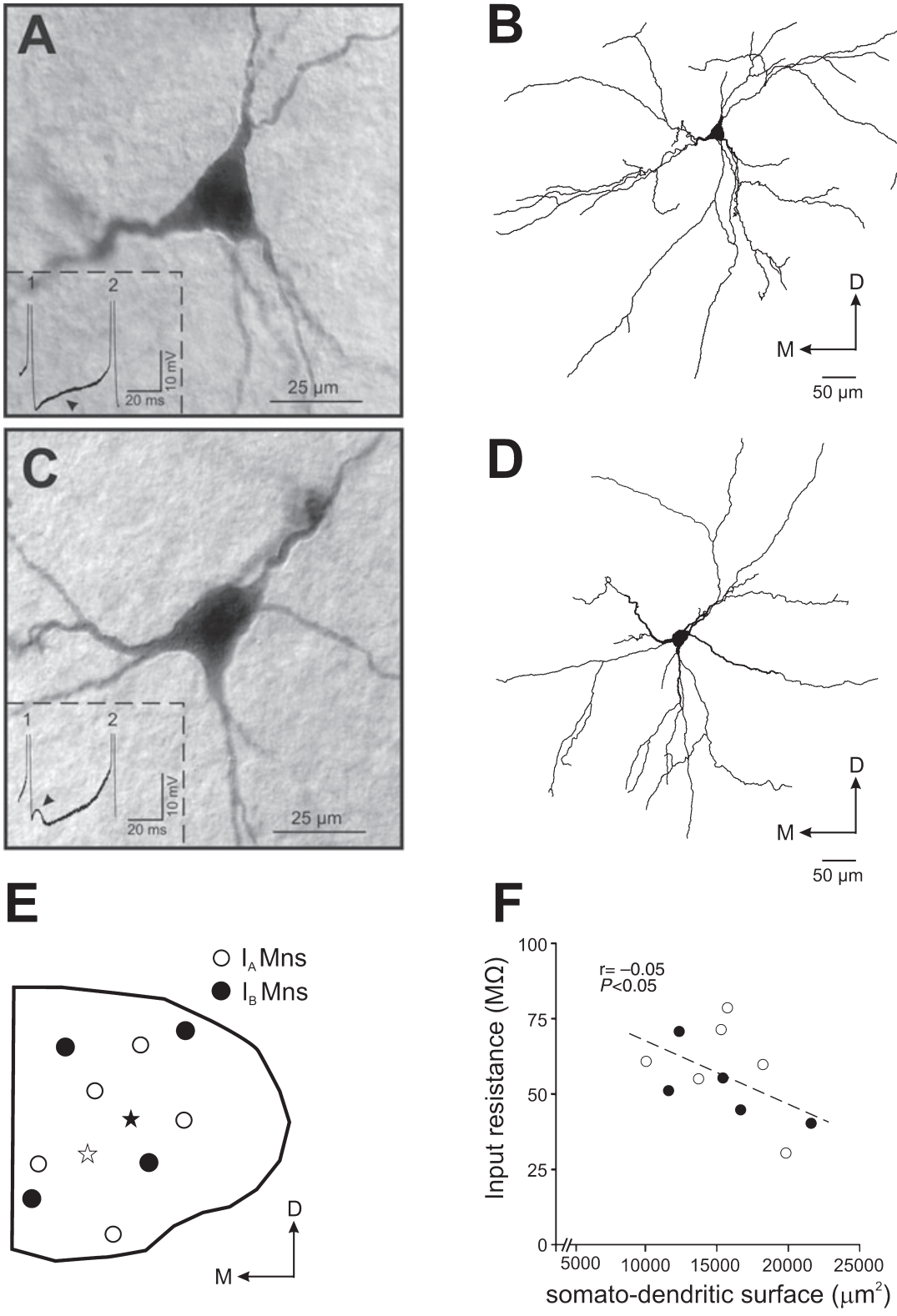

FIG. 7. Anatomical features in I_A and I_B motoneurons (Mns) of the rat oculomotor nucleus. (A–D) Photomicrographs and reconstructions of representative I_A (A and B) and I_B Mns (C and D). The insets show the afterhyperpolarization phase (AHP) between two truncated action potentials (1 and 2) taken from steady state firing for the illustrated neurobiotin-labelled Mns. Arrowheads indicate the AHP concave voltage trace in I_A Mn and the afterdepolarization phase in the I_B Mn. (E) Schematic drawing of a transverse view of the oculomotor nucleus to illustrate the location of intracellularly labelled I_A (○) and I_B (●) Mns within the boundaries of the nucleus. Stars indicate the location of the Mns illustrated in A (unfilled) and C (filled). (F) Plot showing the relationship between somato-dendritic surface and input resistance. Open and filled circles represent the raw data in I_A and I_B Mns, respectively; the dashed line is the best fit to the raw data. D, M are dorsal and medial, respectively.

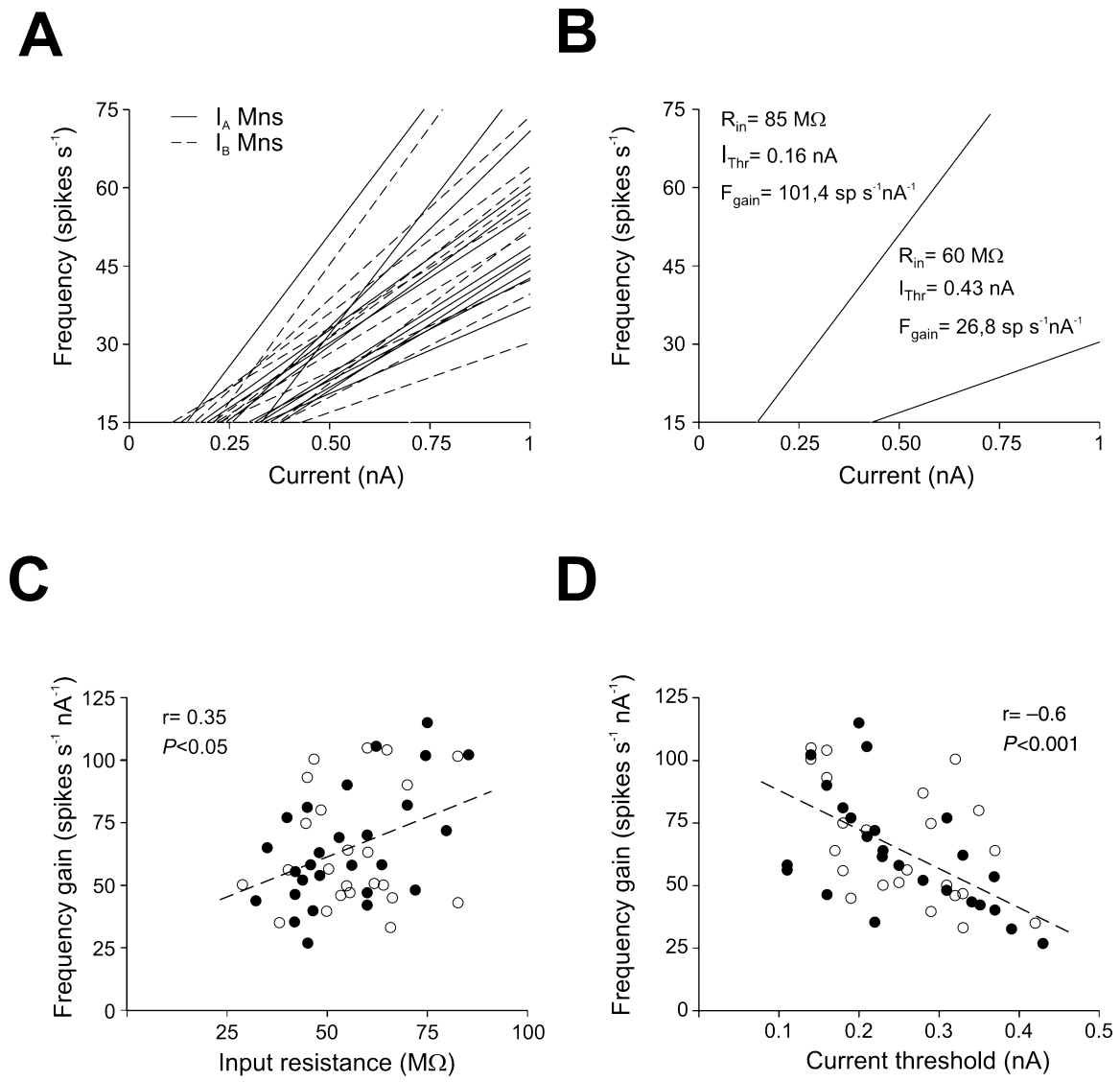

FIG. 8. Frequency in the steady state vs. current intensity (*F/I*) plots as function of the intrinsic membrane properties in I_A and I_B motoneurons (Mns) of the rat oculomotor nucleus. (A) Plot showing the regression lines of the frequency in the steady state for I_A (solid line) and I_B Mns (dashed line) Mns vs. current intensity. The slopes of these *F/I* relationships represent the frequency gain. (B) Graph illustrating the two extreme *F/I* relationship slopes (i.e. frequency gain) found in the present study. In the graph are also indicated the values of frequency gain (F_{gain}), input resistance (R_{in}), and intensity in current threshold (I_{Thr}) for each case. (C and D) Relationship between frequency gain and input resistance (C) or current threshold (D) in I_A and I_B Mns. Open and filled circles represent the raw data in I_A and I_B Mns, respectively; the dashed lines are the best fit to the raw data. sp, spike.

Types II, III, and IV Mns

Type II Mns failed to maintain their repetitive discharge longer than 300 ms after stimulus onset. We found type II Mns in lower percentages, in both neonatal and adult periods, than did earlier works (Gueritaud, 1988; Tsuzuki *et al*., 1995). Furthermore, this repetitive discharge pattern has also been identified in abducens, spinal cord, and facial Mns (Fulton & Walton, 1986; Durand, 1989a; Magarinos-Ascone *et al*., 1999), as well as in other nuclei (Saito & Isa, 1999; Ruscheweyh & Sandkühler, 2002; Straka *et al*., 2004; Laursen & Rekling, 2006). Type III Mns were recorded exclusively in the neonatal period, and showed a sustained repetitive discharge that began with a delay in relation to the stimulus onset. This type of repetitive discharge has already been reported in the neonatal abducens Mns (Russier *et al*., 2003) and other structures (Saito & Isa, 1999; Ruscheweyh & Sandkühler, 2002). Type IV Mns discharged bursts of spikes distributed discontinuously during the depolarizing current steps. A similar discharge pattern has been reported in prepositus hypoglossi nucleus (Idoux *et al*., 2006), cortex, and spinal cord neurons (Kawaguchi, 1995; Cauli *et al*., 1997; Ruscheweyh & Sandkühler, 2002), but, to our knowledge, never in a motoneuronal pool. In functional terms, it should be remarked first that type III Mns were confined to the neonatal period (i.e. presented an immature discharge rate, Russier *et al*., 2003), and types II and IV Mns were rare in the adult (lower than 10% of recorded Mns) and not reported in alert preparation; second, neurons with transient discharge (such as the type II Mns reported here) reach a sustained firing rate as a function of the stimulation of cholinergic inputs (Magarinos-Ascone *et al*., 1999) or by modifications in potassium conductances induced by repetitive depolarizing stimulation (Laursen & Rekling, 2006); third, type IV Mns exhibited a sustained discharge at high current intensity. Taking all these data together, we conclude that the

participation of type II and IV Mns in eye movements in the adult would be uncertain, requiring clarification in future research.

Type I Mns

Type I Mns were the most abundant in both the neonatal and adult periods (approximately 90%). They showed a sustained discharge throughout the current step. Earlier works reported this pattern of discharge, although in lower proportion, in both oculomotor and abducens Mns (Gueritaud, 1988; Tsuzuki *et al*., 1995; Russier *et al*., 2003). A similar repetitive firing has also been reported in all motoneuronal pools studied (Fulton & Walton, 1986; Nunez-Abades *et al*., 1993; Chandler *et al*., 1994; Viana *et al*., 1995; Magarinos-Ascone *et al*., 1999). In addition, superior colliculus (Saito & Isa, 1999) and vestibular nuclei (Serafin *et al*., 1991; Johnston *et al*., 1994) neurons exhibit a sustained discharge.

We provide here evidence for the first time in the oculomotor nucleus to distinguish between I_A and I_B Mns as a function of the action-potential shape and firing response to current steps. I_A Mns showed a single AHP, while I_B Mns exhibited an initial fast AHP, followed by a delayed slow AHP. Furthermore, I_B Mns showed an afterdepolarization phase. In addition, the amplitude of the action potential was similar in I_A and I_B Mns, while its duration was significantly longer for I_A Mns as a consequence of slower kinetics in the falling phase. With similar findings, earlier works also divided vestibular neurons into these two categories (Serafin *et al*., 1991; Johnston *et al*., 1994; Him & Dutia, 2001; Beraneck *et al*., 2003). In vestibular neurons, the combination of electrophysiological and pharmacological studies has distinguished different potassium and calcium conductances shaping the falling and AHP phases of the action potential (reviewed in Darlington *et al*., 1995; Peusner *et al*., 1998; Straka *et al*., 2005). Whether such conductances are also underlying I_A and I_B Mns of the rat oculomotor nucleus is not known.

It has been proposed that A and B neurons in vestibular nuclei are two separate populations, or part of a functional continuum (du Lac & Lisberger, 1995; Straka *et al*., 2005), although it transpires that such proposals are not mutually exclusive (Beraneck *et al*., 2003; Sekirnjak & du Lac, 2006; see also Straka *et al*., 2005). Consequently, are I_A and I_B two motoneuronal populations, or part of a functional continuum? The firing properties of these Mns could provide support for both proposals. In fact, the raw data of the initial adaptation index (Fig. 4A) and the *F/I* plots for the first interspike interval (Fig. 6C and D) changed in a continuum for I_A and I_B Mns. However, they were shifted in such a way that we could score functional differences between I_A and I_B Mns (see for example the results of the maximum frequency plot). In addition, the presence of ocular Mns with similar features to those in vestibular nuclei leads to the query of whether these two types of neuron are separate connections, for instance, are I_A Mns primarily targeted by type A vestibular neurons?

F/I plots and phasic firing – functional consequences

It is currently accepted that ocular Mns exhibit a burst of spikes – phasic firing – correlated with saccadic eye velocity, and a steady firing – tonic firing – associated to eye position (Delgado-Garcia *et al*., 1986; Fuchs *et al*., 1988; de la Cruz *et al*., 1989; Pastor & Gonzalez-Forero, 2003). The pulse-slide-step discharge of Mns is produced by separate premotor neurons in the rostral midbrain, pons, and medulla. The pulse signal determines eye saccade duration, amplitude, and velocity (reviewed in Scudder *et al*., 2002; Sparks, 2002). Cognizant that a one-second step of depolarizing current produces a change in frequency more closely resembling a step than pulse-slide-step (Remmel & Marrocco, 1975), we studied the phasic firing in I_A and I_B Mns after stimulus onset. I_A Mns in response to current steps up to 0.5 nA exhibited an instantaneous frequency during the first interval interspike similar to those in the steady state (tonic firing), while the response shifted to phasic-tonic for higher-current stimuli. In contrast, I_B Mns showed a phasic-tonic firing irrespective of the current intensity. Second, the first interspike interval reached frequencies always significantly higher for I_B than for I_A Mns, i.e. the phasic firing was more pronounced in I_B Mns. Third, the dynamic firing range was narrower for I_A Mns (0.1–2 nA) than for I_B (0.05–3 nA). Fourth, the range of current intensity that evoked the maximum frequencies in I_A Mns (0.5–2 nA) was lower than in I_B Mns (1–3 nA); consequently, the range of maximum frequencies reached by I_A Mns was lower than that reached by I_B Mns.

These results could be interpreted in the context that Mns represent the final common path for muscle motor innervation. These Mns send their signals to extraocular muscles for executing saccadic eye movements as a 'pulse'; such a command is required to overcome the resistance of viscous drag of the orbital tissue for executing saccades (Robinson, 1970). According to this idea, and as I_A and I_B Mns showed differences in the phasic firing, these Mns could contribute differently to the pulse and therefore to saccadic eye movements. Extraocular muscle expresses all known striated muscle isoforms of myosin heavy chain (Spencer & Porter, 2006), and we suggest that I_A and I_B Mns could innervate fast-twitch muscle fibres with different contraction speed. However, the raw data for frequency of the first interspike interval indicated that between the two canonical functional I_A and I_B Mns, there was a continuum of phasic firing (see Fig. 6B and C); these data could also be consistent with the notion that the aggregate population of singly innervated fibres in extraocular muscle may form a continuum of fast-twitch fibres differing in contraction speed and fatigability (Nelson *et al*., 1986). We conclude that even though each oculomotor nucleus Mn would receive identical pulse synaptic input from premotor neurons, their intrinsic membrane properties could contribute to generating a fine phasic firing for a graded muscle contraction.

Are type I_A and I_B Mns a substratum to innervate singly and multiply innervated extraocular muscle fibres? Mns projecting to non-twitch or multiply innervated fibres have smaller somata than those projecting to twitch or singly innervated fibres, and they cluster at or close to the medial border, although in rat some of them are scattered within the oculomotor nucleus (Eberhorn *et al*., 2006). Immunohistochemical studies have revealed differences between Mns innervating twitch and non-twitch muscle fibres (Eberhorn *et al*., 2005, 2006). Furthermore, multiply innervated muscle fibres are not suited to contributing significantly to saccadic eye movements, but are more suited to playing a role in eye fixations (Dean, 1996; Büttner-Ennever *et al*., 2001). In fact, it has been reported that following eye saccades, rats are able to maintain a steady eye position for long periods (Chelazzi *et al*., 1989). As I_A Mns could show a tonic discharge, we wondered if they were neuronal substratum innervating non-twitch muscle fibres. According to our sampling, I_A and I_B Mns were intermingled within the boundaries of the oculomotor nucleus, and they had similarly sized somata. Therefore, we conclude that I_A Mns, considered as a unique pool, do not constitute a probable anatomical substratum to innervate non-twitch muscle fibres. However, a combination of electrophysiological, anatomical, and immunohistochemical techniques would be required to elucidate whether some of the I_A Mns could innervate the non-twitch muscle fibres.

F/I plots and tonic firing: size principle and recruitment thresholds

In addition to the pulse signal, the Mns discharge a 'step' (Robinson, 1970), i.e. a tonic discharge which is proportional to eye position, and balances the elastic forces that would otherwise return the eye to its primary position after termination of the pulse. According to our results on tonic firing, we suggest that both I_A and I_B Mns could contribute similarly to eye fixations. Alert preparation studies have shown that Mns begin to fire when the eye position reaches a threshold value in the on-direction. Above this threshold, the firing rate varies linearly with eye position, with slope *K* (Delgado-Garcia *et al*., 1986; Fuchs *et al*., 1988; de la Cruz *et al*., 1989). Some of these studies have suggested that the parameter *K* and input resistance are related (Delgado-Garcia *et al*., 1986; Pastor & Gonzalez-Forero, 2003). It is widely accepted that recruitment threshold values and *K* are related; Mns with higher threshold have greater slope *K* (Delgado-Garcia *et al*., 1986; Fuchs *et al*., 1988; de la Cruz *et al*., 1989; Van Gisbergen & Van Opstal, 1989). Current proposals suggest that the above-mentioned differences in slope *K* between Mns might be determined either by the intrinsic membrane properties of the Mns, or by differences in synaptic inputs to them, or by a combination of the two (Dean, 1997). To test these hypotheses, we explored whether the firing-rate gain (which mimics in slice preparation the slope *K* in alert studies) is related with input resistance or recruitment threshold.

Our data demonstrated a significant relationship between size and input resistance, i.e. smaller Mns had higher input resistance. There was also a significant relationship between firing-rate gain and input resistance, consistent with previous data (Grantyn & Grantyn, 1978), but with a poor linear regression. These data lead to the conclusion that the size principle (Henneman *et al*., 1965) has to be tempered in its contribution to firing-rate gain, and additional mechanisms would be required. *In vivo* studies also raise doubts about the contribution of the size principle in the recruitment threshold of Mns and their *K* slopes. In fact, some of them have also found a weak relationship between size – inferred from the latency to elicit a spike antidromically – and slope K (Delgado-Garcia *et al*., 1986; Pastor & Gonzalez-Forero, 2003), while others did not find any relationship (Fuchs *et al*., 1988). Therefore, present data agree with the suggestion that a recruitment order based exclusively on a size principle seems not to be a sufficient criterion for ranking the motoneuronal pool as a function of firing-related parameters (Pastor *et al*., 1991).

As already mentioned, eye-position recruitment threshold of the Mns, which in turn determines *K*, could depend on membrane intrinsic properties and/or synaptic inputs (Dean, 1997; Hazel *et al*., 2002; Pastor & Gonzalez-Forero, 2003). Following the common drive model, if each Mn receives identical afferent inputs, differences between the resultant firing rates are caused by differences in the intrinsic properties of the Mns (De Luca & Erim, 1994; Dean, 1997). Present results show an inverse relationship between frequency gain and current threshold. Consistent with this proposal, an early work also demonstrated a negative relationship between rheobase and frequency gain (Grantyn & Grantyn, 1978). Therefore, we rule out the common drive model as the sole mechanism determining threshold and frequency gain. In addition, synaptic inputs have been suggested as determinant for establishing the recruitment threshold (Hazel *et al*., 2002; Pastor & Gonzalez-Forero, 2003), and many conductances subject to control by neuromodulators are important for the production of appropriate rates of repetitive firing in other motoneuronal pools (Bayliss *et al*., 1992; Berger *et al*., 1992; Heckman *et al*., 2003; Fedirchuk & Dai, 2004; Brownstone, 2006). From all these data, we conclude that intrinsic membrane properties could not support the covariation between tonic firing gain and recruitment thresholds reported in alert studies, which suggests that synaptic inputs play a primary role.

Acknowledgements

This work was supported by Spanish MEC (BFU2006-08895) grant. We would like to thank the anonymous reviewers; their commenteries greatly strengthened this manuscript.

Abbreviations

AHP, afterhyperpolarization; Mns, motoneurons.

References

Bayliss, D.A., Viana, F. & Berger, A.J. (1992) Mechanisms underlying excitatory effects of thyrotropin-releasing hormone on rat hypoglossal motoneurons *in vitro*. *J. Neurophysiol.*, **68**, 1733–1745.

Beraneck, M., Hachemaoui, M., Idoux, E., Ris, L., Uno, A., Godaux, E., Vidal, P.P., Moore, L.E. & Vibert, N. (2003) Long-term plasticity of ipsilesional medial vestibular nucleus neurons after unilateral labyrinthectomy. *J. Neurophysiol.*, **90**, 184–203.

Berger, A.J., Bayliss, D.A. & Viana, F. (1992) Modulation of neonatal rat hypoglossal motoneuron excitability by serotonin. *Neurosci. Lett.*, **143**, 164–168.

Brownstone, R.M. (2006) Beginning at the end: repetitive firing properties in the final common pathway. *Prog. Neurobiol.*, **78**, 156–172.

Burgoon, P.W. & Boulant, J.A. (2001) Temperature-sensitive properties of rat suprachiasmatic nucleus neurons. *Am. J. Physiol. Regul. Integr. Comp. Physiol.*, **281**, 706–715.

Büttner-Ennever, J.A., Horn, A.K., Scherberger, H. & D'Ascanio, P. (2001) Motoneurons of twitch and nontwitch extraocular muscle fibers in the abducens, trochlear, and oculomotor nuclei of monkeys. *J. Comp. Neurol.*, **438**, 318–335.

Carpenter, R.H.S. (1988) *Movements of the Eyes*. Pion, London.

Carrascal, L., Nieto-Gonzalez, J.L., Cameron, W.E., Torres, B. & Nunez-Abades, P.A. (2005) Changes during the postnatal development in physiological and anatomical characteristics of rat motoneurons studied *in vitro*. *Brain Res. Rev.*, **49**, 377–387.

Carrascal, L., Nieto-Gonzalez, J.L., Nunez-Abades, P. & Torres, B. (2006) Temporal sequence of changes in electrophysiological properties of oculomotor motoneurons during postnatal development. *Neuroscience*, **140**, 1223–1237.

Cauli, B., Audinat, E., Lambolez, B., Angulo, M.C., Ropert, N., Tsuzuki, K., Hestrin, S. & Dossier, J. (1997) Molecular and physiological diversity of cortical nonpyramidal cells. *J. Neurosci.*, **17**, 3894–3906.

Chandler, S.H., Saio, H., Inoue, T. & Goldberg, L.J. (1994) Electrophysiological properties of guinea pig trigeminal motoneurons recorded *in vitro*. *J. Neurophysiol.*, **71**, 129–145.

Chelazzi, L., Rossi, F., Tempia, F., Ghirardi, M. & Strata, P. (1989) Saccadic eye movements and gaze holding in the head-restrained pigmented rat. *Eur. J. Neurosci.*, **1**, 639–646.

Darlington, C.L., Gallagher, J.P. & Smith, P.F. (1995) *In vitro* electrophysiological studies of the vestibular nucleus complex. *Prog. Neurobiol.*, **45**, 335–346.

de la Cruz, R.R., Escudero, M. & Delgado-Garcia, J.M. (1989) Behaviour of medial rectus motoneurons in the alert cat. *Eur. J. Neurosci.*, **1**, 288–295.

De Luca, C.J. & Erim, Z. (1994) Common drive of motor units in regulation of muscle force. *TINS*, **17**, 299–305.

Dean, P. (1996) Motor unit recruitment in a distributed model of extraocular muscle. *J. Neurophysiol.*, **76**, 727–742.

Dean, P. (1997) Simulated recruitment of medial rectus motoneurons by abducens internuclear neurons: synaptic specificity vs. intrinsic motoneuron properties. *J. Neurophysiol.*, **78**, 1531–1549.

Delgado-Garcia, J.M., del Pozo, F. & Baker, R. (1986) Behavior of neurons in the abducens nucleus of the alert cat. I. Motoneurons. *Neuroscience*, **17**, 929–952.

Durand, J. (1989a) Electrophysiological and morphological properties of rat abducens motoneurones. *Exp. Brain Res.*, **76**, 141–142.

Durand, J. (1989b) Intracellular study of oculomotor neurons in the rat. *Neuroscience*, **30**, 639–649.
Eberhorn, A.C., Ardeleanu, P., Buttner-Ennever, J.A. & Horn, A.K. (2005) Histochemical differences between motoneurons supplying multiply and singly innervated extraocular muscle fibers. *J. Comp. Neurol.*, **491**, 352–366.
Eberhorn, A.C., Büttner-Ennever, J.A. & Horn, A.K. (2006) Identification of motoneurons supplying multiply- or singly-innervated extraocular muscle fibers in the rat. *Neuroscience*, **137**, 891–903.
Fedirchuk, B. & Dai, Y. (2004) Monoamines increase the excitability of spinal neurones in the neonatal rat by hyperpolarizing the threshold for action potential production. *J. Physiol.*, **557**, 355–361.
Fuchs, A.F. & Luschei, E.S. (1971) The activity of single trochlear nerve fibers during eye movements in the alert monkey. *Exp. Brain Res.*, **13**, 78–89.
Fuchs, A.F., Scudder, C.A. & Kaneko, C.R. (1988) Discharge patterns and recruitment order of identified motoneurons and internuclear neurons in the monkey abducens nucleus. *J. Neurophysiol.*, **60**, 1874–1895.
Fulton, B.P. & Walton, K. (1986) Electrophysiological properties of neonatal rat motoneurons studied *in vitro*. *J. Physiol.*, **370**, 651–678.
Gallagher, J.P., Lewis, M.R. & Galagher, P.S. (1985) An electrophysiological investigation of the rat medial vestibular nucleus *in vitro*. *Prog. Clin. Biol. Res.*, **176**, 293–304.
Grantyn, R. & Grantyn, A. (1978) Morphological and electrophysiological properties of cat abducens motoneurons. *Exp. Brain Res.*, **15**, 249–274.
Gueritaud, J.P. (1988) Electrical activity of rat ocular motoneurons recorded *in vitro*. *Neuroscience*, **24**, 837–852.
Hazel, T.R., Sklavos, S.G. & Dean, P. (2002) Estimation of premotor synaptic drives to simulated abducens motoneurons for control of eye position. *Exp. Brain Res.*, **146**, 184–196.
Heckman, C.J., Lee, R.H. & Brownstone, R.M. (2003) Hyperexcitable dendrites in motoneurons and their neuromodulatory control during motor behavior. *TINS*, **26**, 688–695.
Henneman, E., Somjen, G. & Carpenter, D.O. (1965) Functional significance of cell size in spinal motoneurons. *J. Neurophysiol.*, **28**, 560–580.
Him, A. & Dutia, M.B. (2001) Intrinsic excitability changes in vestibular nucleus neurons after unilateral deafferentation. *Brain Res.*, **908**, 58–66.
Idoux, E., Serafin, M., Fort, P., Vidal, P.P., Beraneck, M., Vibert, N., Muhlethaler, M. & Moore, L.E. (2006) Oscillatory and intrinsic membrane properties of guinea pig nucleus prepositus hypoglossi neurons *in vitro*. *J. Neurophysiol.*, **96**, 175–196.
Johnston, A.R., MacLeod, N.K. & Dutia, M.B. (1994) Ionic conductances contributing to spike repolarization and after-potentials in rat medial vestibular nucleus neurones. *J. Neurophysiol.*, **481**, 61–77.
Kawaguchi, Y. (1995) Physiological subgroups of nonpyramidal cells with specific morphological characteristics in layer II/III of rat frontal cortex. *J. Neurosci.*, **15**, 2638–2655.
Keller, E.L. (1981) Oculomotor neuron behavior. In Zuber, B.L., (Ed) *Models of Oculomotor Behavior and Control.* CRC Press, Boca Raton, Florida, pp. 1–19.
du Lac, S. & Lisberger, S.G. (1995) Membrane and firing properties of avian medial vestibular nucleus neurons *in vitro*. *J. Comp. Physiol. [a]*, **176**, 641–651.
Laursen, M. & Rekling, J.C. (2006) The Edinger-Westphal nucleus of the juvenile rat contains transient- and repetitive-firing neurons. *Neuroscience*, **141**, 191–200.
Magarinos-Ascone, C., Nunez, A. & Delgado-Garcia, J.M. (1999) Different discharge properties of rat facial nucleus motoneurons. *Neuroscience*, **94**, 879–886.
Nelson, J.S., Goldberg, S.J. & McClung, J.R. (1986) Motoneuron electrophysiological and muscle contractile properties of superior oblique motor units in cat. *J. Neurophysiol.*, **55**, 715–726.
Nunez-Abades, P.A., He, F., Barrionuevo, G. & Cameron, W.E. (1994) Morphology of developing rat genioglossal motoneurons studied *in vitro*: changes in length, branching pattern, and spatial distribution of dendrites. *J. Comp. Neurol.*, **339**, 401–420.
Nunez-Abades, P.A., Spielmann, J.M., Barrionuevo, G. & Cameron, W.E. (1993) *In vitro* electrophysiology of developing genioglossal motoneurons in the rat. *J. Neurophysiol.*, **70**, 1401–1411.
Pastor, A.M. & Gonzalez-Forero, D. (2003) Recruitment order of cat abducens motoneurons and internuclear neurons. *J. Neurophysiol.*, **90**, 2240–2252.
Pastor, A.M., Torres, B., Delgado-Garcia, J.M. & Baker, R. (1991) Discharge characteristics of medial rectus and abducens motoneurons in the goldfish. *J. Neurophysiol.*, **66**, 2125–2140.
Peusner, K.D., Gramkrelidze, G. & Giaume, C. (1998) Potassium currents and excitability in second-order auditory and vestibular neurons. *J. Neurosci. Res.*, **53**, 511–520.
Rekling, J.C., Funk, G.D., Bayliss, D.A., Dong, X.W. & Feldman, J.L. (2000) Synaptic control of motoneuronal excitability. *Physiol. Rev.*, **80**, 767–852.
Remmel, R.S. & Marrocco, R.T. (1975) Impulse generation properties of abducens motoneurons. *Vis. Res.*, **15**, 1039–1043.
Robinson, D.A. (1970) Oculomotor unit behavior in the monkey. *J. Neurophysiol.*, **33**, 393–403.
Ruscheweyh, R. & Sandkühler, J. (2002) Lamina-specific membrane and discharge properties of rat spinal dorsal horn neurones *in vitro*. *J. Physiol.*, **541**, 231–244.
Russier, M., Carlier, E., Ankri, N., Fronzaroli, L. & Debanne, D. (2003) A-, T-, and H-type currents shape intrinsic firing of developing rat abducens motoneurons. *J. Physiol.*, **549**, 21–36.
Saito, Y. & Isa, T. (1999) Electrophysiological and morphological properties of neurons in the rat superior colliculus. I. Neurons in the intermediate layer. *J. Neurophysiol.*, **82**, 754–767.
Sawczuk, A., Powers, R.K. & Binder, M.D. (1995) Spike frequency adaptation studied in hypoglossal motoneurons of the rat. *J. Neurophysiol.*, **73**, 1799–1810.
Scudder, C.A., Kaneko, C.S. & Fuchs, A.F. (2002) The brainstem burst generator for saccadic eye movements: a modern synthesis. *Exp. Brain Res.*, **142**, 439–462.
Sekirnjak, C. & du Lac, S. (2006) Physiological and anatomical properties of mouse medial vestibular nucleus neurons projecting to the oculomotor nucleus. *J. Neurophysiol.*, **95**, 3012–3023.
Serafin, M., de Waele, C., Khateb, A., Vidal, P.P. & Mühlethaler, M. (1991) Medial vestibular nucleus in the guinea-pig. I. Intrinsic membrane properties in brainstem slices. *Exp. Brain Res.*, **84**, 417–425.
Sparks, D.L. (2002) The brainstem control of saccadic eye movements. *Nature Rev. Neurosci.*, **3**, 952–964.
Spencer, R.F. & Porter, J.D. (2006) Biological organization of the extraocular muscles. In Büttner-Ennever, J.A., (Ed.), *Neuroanatomy of the Oculomotor System. Progress in Brain Research*, **Vol. 151**. Elsevier, Amsterdam. pp. 43–80.
Stahl, J.S. & Simpson, J.I. (1995) Dynamics of abducens nucleus neurons in the awake rabbit. *J. Neurophysiol.*, **73**, 1383–1395.
Straka, H., Beraneck, M., Rohregger, M., Moore, L.E., Vidal, P.P. & Vibert, N. (2004) Second-order vestibular neurons form separate populations with different membrane and discharge properties. *J. Neurophysiol.*, **92**, 845–861.
Straka, H., Vibert, N., Vidal, P.P., Moore, L.E. & Dutia, M.B. (2005) Intrinsic membrane properties of vertebrate vestibular neurons: function, development and plasticity. *Prog. Neurobiol.*, **76**, 349–392.
Sylvestre, P.A. & Cullen, K.E. (1999) Quantitative analysis of abducens neuron discharge dynamics during saccadic and slow eye movements. *J. Neurophysiol.*, **82**, 2612–2632.
Thompson, S.M., Masukawa, L.M. & Prince, D.A. (1985) Temperature dependence of intrinsic membrane properties and synaptic potentials in hippocampal CA1 neurons *in vitro*. *J. Neurosci.*, **5**, 817–824.
Tsuzuki, S., Yoshida, S., Yamamoto, T. & Oka, H. (1995) Developmental changes in the electrophysiological properties of neonatal rat of oculomotor neuron studied *in vitro*. *Neurosci. Res.*, **23**, 389–397.
Van Gisbergen, J.A. & Van Opstal, A.J. (1989) Models. In Goldberg, M.E. & Wurtz, R.H., (Eds), *The Neurobiology of Saccadic Eye Movements. Reviews of oculomotor research 3.* Elsevier, Amsterdam, pp. 69–101.
Viana, F., Bayliss, D.A. & Berger, A.J. (1995) Repetitive firing properties of developing rat brainstem motoneurons. *J. Physiol.*, **486**, 745–761.
Zhao, Y. & Boulant, J.A. (2005) Temperature effects on neuronal membrane potentials and inward currents in rat hypothalamic tissue slices. *J. Physiol.*, **564**, 245–257.